Structures and Lagrangian statistics of the Taylor-Green Dynamo

H Homann[1], Y Ponty[1], G Krstulovic[1], R Grauer[2]

[1] Université de Nice-Sophia, CNRS, Observatoire de la Côte d'Azur, CS 34229, 06304 Nice Cedex 4, France

[2] Institut für Theoretische Physik I, Ruhr-Universität Bochum, 44780 Bochum, Germany

Abstract. The evolution of a Taylor-Green forced magnetohydrodynamic (MHD) system showing dynamo activity is analyzed via direct numerical simulations. The statistical properties of the velocity and magnetic field in Eulerian coordinates and along trajectories of fluid elements (Lagrangian coordinates) are found to change between the kinematic, non-linear and saturated regime. Fluid element (tracer) trajectories change from chaotic quasi-isotropic (kinematic phase) to mean magnetic field aligned (saturated phase). The probability density functions (PDFs) of the magnetic field change from strongly non-Gaussian in the kinematic to quasi-Gaussian PDFs in the saturated regime so that their flatness give a precise handle on the definition of the limiting points of the three regimes. Also the statistics of the fluctuations of the kinetic and magnetic energy along fluid trajectories change. All this goes along with a dramatic increase of the correlation time of velocity and magnetic field fluctuations experienced by tracers significantly exceeding one turbulent large-eddy turn-over time. A remarkable consequence is an intermittent scaling regime of the Lagrangian magnetic field structure functions at unusually long time scales.

1. introduction

The magnetic field of stars and telluric planets is explained by the dynamo instability, produced by a turbulent conducting fluid, where the induction due to the motion takes over the magnetic diffusion. A system with dynamo action passes through different stages from the linear (kinematic) to the non-linear and finally to the saturated phase. During the kinematic phase the magnetic energy grows exponentially but has no influence on the flow. During the non-linear phase the Lorentz force changes the flow and at the saturation state the diffusion and the electromotive force reach an equilibrium. The system reaches the fully non-linear magnetohydrodynamic (MHD) regime, driven by an energy exchange between the velocity and magnetic field.

In the last decade, several experimental groups have investigated dynamo action in laboratory experiments using liquid sodium [1, 2, 3, 4, 5, 6]. The instability threshold and a rich non-linear behavior along the saturation regime have been largely observed [7, 8, 9, 10]. Investigations of the fast kinematic dynamo [11] in the 90's, showed the important role of the chaotic properties of the fluid trajectories for the dynamo threshold. The effect of turbulent fluctuations on the dynamo onset has also been studied in Navier-Stokes flows [12, 13] and some noisy models [14], distinguishing the important role between the mean flow dynamo and fluctuation dynamo modes [15].

The transition between the linear and the saturation regime has been studied measuring the finite-time Lyapunov exponent of the flow trajectories [16, 17]. These results showed a strong reduction of the chaotic properties in the saturation phase, due to the action of the Lorentz force. Fluid trajectories thus change along the different dynamo phases. This naturally motivates the use of a Lagrangian description where the properties of the flow are investigated by using tracers [18].

Lagrangian statistics describe the dynamical evolution of physical quantities along tracer trajectories in contrast to the Eulerian perspective in which such quantities are analyzed on fixed spatial points. During the last decades Lagrangian studies revealed new aspects of homogeneous and isotropic turbulence [19]. The trajectory point of view proved useful especially for the study of coherent structures and intermittency [20, 21, 22] as well as for diffusion and dispersion properties of hydrodynamic and MHD homogeneous and isotropic turbulence [23, 24, 25]. This approach has produced many experimental results by tracking solid inertial particles or bubbles [26, 27, 28, 29], which can have a different dynamics compared to simple tracers. Lagrangian statistics has also been used in MHD simulations [30, 31] to compare the anomalous exponents of the structure function to their hydrodynamic counterparts and to understand the relation between Eulerian and Lagrangian statistics.

In this study we use a Lagrangian approach in the context of turbulent dynamo action. In the Kraichnan-Kazantsev framework it served to determine the dynamo onset as a function of the roughness of the flow [32]. In this work the Lagrangian perspective allows us to precisely define the limiting points of each regime, to highlight the correlation of the magnetic field and the fluid trajectories and to discover a to our

knowledge unknown scaling regime at time scales well beyond the large-eddy turn-over time of the turbulent flow.

The dynamo systems under consideration in this work is induced mainly by the so called Taylor-Green forcing [33]. For comparison, a second forcing where the large scales of the velocity field are frozen in time is also considered. The Taylor-Green flow, which can produce dynamo action, is a very well documented study case involving rich dynamo behaviors in both the linear and the non-linear regime [34, 35, 36, 37, 12, 14, 38, 39]. The Taylor-Green flow contained in a periodic box has several properties that mimic the von Kàrmàn flow, driven by two counter-rotating impellers. The von Kàrmàn flow has a strong experimental history inside the turbulent and the dynamo scientific communities. Indeed, several teams set up such experiments with different designs in incompressible [40, 41] and compressible flows [42, 43, 44, 45, 46, 47]. This type of experiment was also one of the first setup used to study Lagrangian statistics of turbulent flows [26, 27, 28, 29]. After the intensive water campaign experiments of the Saclay group [48, 49, 50, 51, 52], this setup has lead to the von Kàrmàn Sodium (VKS) dynamo campaigns also cited above.

This paper is organized as follows: In the next section the dynamo system under consideration and the numerical method are explained. In section 3 the evolution of the flow structure and trajectories within the three different regimes are discussed. Section 4 investigates the consequences for the velocity and magnetic field fluctuations. A magnetic field scaling regime at very large temporal scales is presented in section 5. Conclusions are drawn in section 6.

2. Model and methods

We perform direct numerical simulations of turbulent MHD flows with large-scale forcing in a periodic box. We integrate the three-dimensional incompressible MHD equations that, expressed in Alfvénic units, read

$$\partial_t \boldsymbol{u} + \boldsymbol{u}\cdot\nabla\boldsymbol{u} = (\nabla\times\boldsymbol{B})\times\boldsymbol{B} - \nabla p + \nu\nabla^2\boldsymbol{u} + \boldsymbol{F}, \tag{1}$$

$$\partial_t \boldsymbol{B} = \nabla\times(\boldsymbol{u}\times\boldsymbol{B}) + \eta\nabla^2\boldsymbol{B}, \tag{2}$$

$$\nabla\cdot\boldsymbol{u} = 0, \quad \nabla\cdot\boldsymbol{B} = 0, \tag{3}$$

where ν and η are the kinematic viscosity and the magnetic diffusivity respectively. The density of the fluid is set to unity and $\boldsymbol{F}$ is the constant volume force which generates and maintains the turbulent flow. For most simulations (see table 1) we consider the so called Taylor-Green (TG) flow that is generated by forcing with the TG vortex

$$\boldsymbol{F}_{\mathrm{TG}} = F_0\,(\,\sin(k_0x)\cos(k_0y)\cos(k_0z)\,,\,\cos(k_0x)\sin(k_0y)\cos(k_0z)\,,\,0) \tag{4}$$

with $F_0 = 3$ and $k_0 = 1$ or $k_0 = 2$. When $k_0 = 1$, this forcing leads to a subdivision of the total domain in eight fundamental boxes that, when symmetries are preserved, can be related to each other by mirror-symmetric transformations. Each fundamental box contains a swirling flow composed of a shear layer between two counter-rotating

run	regime	Pm	Re	force type	N	N_p
tgH	hydro	-	350	TG ($k_0 = 1$)	256^3	$2 \cdot 10^5$
tg1	saturated	1/4	297	TG ($k_0 = 1$)	256^3	$2 \cdot 10^5$
tg2	saturated	1/2	670	TG ($k_0 = 1$)	256^3	$2 \cdot 10^5$
tg3	saturated	1	676	TG ($k_0 = 1$)	256^3	$2 \cdot 10^5$
tg4	saturated	1	128	TG ($k_0 = 2$)	256^3	$2 \cdot 10^5$
tg5	saturated	1	545	TG ($k_0 = 1$)	128^3	$2 \cdot 10^4$
ffH	hydro	-	476	FF (frozen)	256^3	$2 \cdot 10^5$
ff	saturated	1	625	FF (frozen)	256^3	$2 \cdot 10^5$

Table 1: List of the numerical simulations. $Pm = \nu/\eta$: magnetic Prandtl number, $Re = u^{\rm rms}\, L/\nu$: Reynolds number, $u^{\rm rms}$ root mean square velocity (defined in table 2), N number of collocation points, N_p number of tracer particles.

eddies. The TG flow mimics some aspects of the von Kàrmàn flow, largely used in hydrodynamics turbulence and dynamo action experiments. As we will see in the following sections, the TG dynamo action presents some particular properties due to its anisotropy. In order to distinguish universal and non-universal properties of the TG dynamo action we also consider a mechanical force $\mathbf{F}$ (see run ffH and ff in table 1) obtained by keeping constant all Fourier modes of the velocity field in the two lowest shells (henceforth called frozen force simulation (FF)). This force is much less structured than the TG forcing and the corresponding flow is found to be nearly isotropic.

We use classical global quantities to characterize the different dynamo phases. The kinetic energy $E_{\rm kin}$, the magnetic energy $E_{\rm mag}$, the enstrophy Ω, the cross helicity H_C, and the magnetic helicity H_M are defined as

$$E_{\rm kin} = \frac{1}{2}\left\langle \mathbf{u}^2 \right\rangle \,,\; E_{\rm mag} = \frac{1}{2}\left\langle \mathbf{B}^2 \right\rangle \,,\; \Omega = \frac{1}{2}\langle (\nabla \times \boldsymbol{u})^2 \rangle \,,$$
$$H_C = \langle \mathbf{u} \cdot \mathbf{B} \rangle \,,\; H_M = \langle \mathbf{A} \cdot \mathbf{B} \rangle \,,$$

where $\langle\ \rangle$ stands for spatial average and $\mathbf{B} = \nabla \times \mathbf{A}$ with $\mathbf{A}$ the magnetic potential. In the ideal case ($\nu = \eta = 0$) and without forcing ($\mathbf{F} = 0$), $E_{\rm tot} = E_{\rm kin} + E_{\rm mag}$, H_C and H_M are conserved by the MHD equations.

The TG forcing (4) is purely horizontal, leading to anisotropy in both the hydrodynamic and the MHD regime. In order to quantify this anisotropy we compute the root mean square (rms) values of the perpendicular (xy-plane) and parallel (z) components of the velocity fields and define the global isotropy coefficient ρ_u^{iso} as

$$u_\perp^{\rm rms} = \left[\langle u_x^2 + u_y^2 \rangle/2\,\right]^{1/2} ,\; u_\parallel^{\rm rms} = \langle u_z^2 \rangle^{1/2} \,,$$
$$\rho_u^{iso} = u_\parallel^{\rm rms}/u_\perp^{\rm rms},\; \rho_B^{iso} = B_\parallel^{\rm rms}/B_\perp^{\rm rms}.$$

With these definitions the average rms velocity is $u^{\rm rms} = [(2\,(u_\perp^{\rm rms})^2 + (u_\parallel^{\rm rms})^2)/3]^{1/2}$. We use analog definitions for the magnetic field.

There are also three important dimensionless numbers, namely the kinematic Reynolds number Re, the magnetic Reynolds number Rm and the magnetic Prandtl

run	$u_\perp^{\rm rms}$	$u_\parallel^{\rm rms}$	$B_\perp^{\rm rms}$	$B_\parallel^{\rm rms}$	$\epsilon_{\rm k}$	ρ_u^{iso}	ρ_B^{iso}	l_K	ν	τ_K	L	T_L
tgH	1.74	1.28	-	-	2.26	0.74	-	0.022	0.008	0.060	1.76	1.11
tg1	1.50	0.56	1.86	0.44	1.08	0.37	0.24	0.027	0.008	0.092	1.88	1.49
tg2	1.78	0.63	1.78	0.52	0.94	0.35	0.29	0.027	0.008	0.092	3.58	2.39
tg3	1.87	0.65	1.64	0.56	1.13	0.35	0.34	0.026	0.008	0.086	3.43	2.19
tg4	1.09	0.43	1.04	0.33	0.71	0.39	0.31	0.029	0.008	0.107	1.11	1.2
tg5	1.92	0.63	1.76	0.54	1.23	0.33	0.31	0.03	0.01	0.092	3.38	2.11
ffH	0.14	-	-	-	$1.48 \cdot 10^{-3}$	≈ 1	≈ 1	0.0195	0.0006	0.64	2.0	13.8
ff	0.13	-	0.066	-	$6.4 \cdot 10^{-4}$	≈ 1	≈ 1	0.0243	0.0006	0.99	3.05	24.4

Table 2: Parameters of the numerical simulations. $\epsilon_{\rm k} = 2\nu\langle(\nabla \times \boldsymbol{u})^2\rangle$: mean kinetic energy dissipation rate, $\rho_u^{iso} = u_\parallel^{\rm rms}/u_\perp^{\rm rms}$ isotropy coefficient, $l_K = (\nu^3/\epsilon_{\rm k})^{1/4}$: Kolmogorov dissipation length scale, ν: kinematic viscosity, $\tau_K = (\nu/\epsilon_{\rm k})^{1/2}$: Kolmogorov time scale, $L = (u^{\rm rms})^3/\epsilon_{\rm k}$: integral scale, $T_L = L/u^{\rm rms}$: large-eddy turnover time. For all runs: size of domain $= 2\pi$. For run ffH and ff only the mean rms value of the three components $u_\perp^{\rm rms} = u_\parallel^{\rm rms} = u^{\rm rms}$ is listed which differ by less than 10%.

number Pm defined as

$$Re = \frac{L\, u^{\rm rms}}{\nu}, \quad Rm = \frac{L\, u^{\rm rms}}{\eta}, \quad Pm = \frac{Rm}{Re}. \tag{5}$$

A useful quantity that measures the alignment of velocity and magnetic fields is the normalized cross helicity defined as $h_C = \cos[\mathbf{u}, \mathbf{B}] = H_C/(u^{\rm rms}\, B^{\rm rms})$.

Numerical integration of the MHD equations (1-3) is carried out by using a fully MPI-parallel pseudo-spectral code (LaTu [53]) with a strongly stable third order Runge-Kutta temporal scheme. De-aliasing is performed using the standard 2/3 rule.

In this work we are concerned with the Lagrangian aspects of dynamo action. Lagrangian statistics are obtained by tracers obeying the equations

$$\dot{\boldsymbol{X}}(\boldsymbol{x}, t) = \boldsymbol{v}(t), \quad \boldsymbol{v}(t) = \boldsymbol{u}(\boldsymbol{X}(\boldsymbol{x}, t)), \tag{6}$$

where $\boldsymbol{X}(\boldsymbol{x}, t)$ and $\boldsymbol{v}(t)$ are the position and velocity of a tracer which started $\boldsymbol{x}$ for $t = 0$. The magnetic field along a tracer path is denoted by $\boldsymbol{b}(t) = \boldsymbol{B}(\boldsymbol{X}(\boldsymbol{x}, t))$. The values of the velocity fields and other physical quantities at the particle positions are evaluated and stored using a tricubic interpolation which is numerically efficient and accurate [54]. The equation (6) is integrated with the same third order Runge-Kutta scheme as the equations (1) for the velocity and magnetic fields. Statistical data is obtained from a large number of tracer trajectories varying from $2 \cdot 10^4$ to $2 \cdot 10^6$.

A detailed list of the physical parameters for the different runs is presented in table 2.

3. Dynamo action: structures and trajectories

During dynamo action, three phases are clearly distinguished. The linear phase, where a seed of magnetic field grows exponentially by the dynamo instability without back-reaction on the velocity field. The second stage, called the non-linear phase, corresponds

to the one where the Lorentz force starts to act on the flow and the kinetic energy slightly drops by the transfer of kinetic energy to the magnetic field. Finally the full MHD system reaches a statistically stationary state, refereed to as the saturation regime. In Fig. 1 (left) the kinetic and magnetic energy is displayed for the TG flow. The three phases of the dynamo action are separated by dashed vertical lines. In Fig. 1 (right) the enstrophy

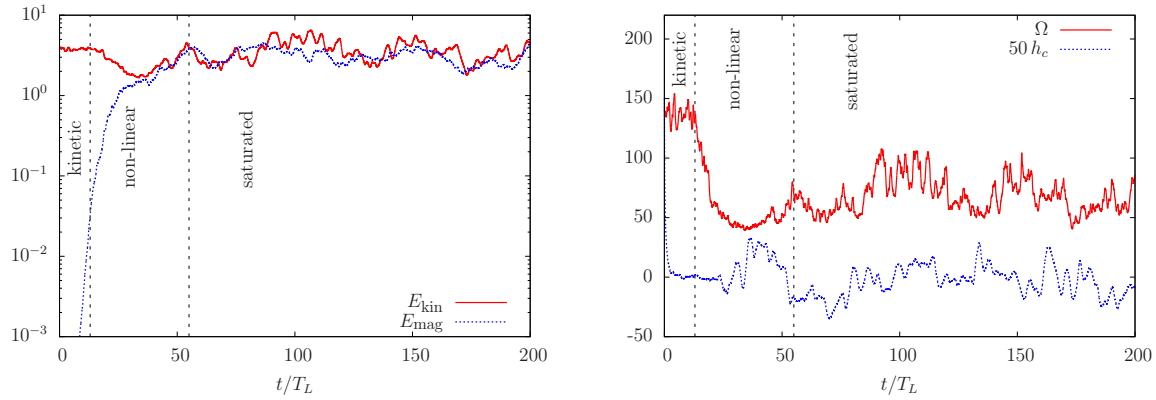


Figure 1: Temporal evolution of kinetic and magnetic energy (left). In the right panel the enstrophy and normalized cross helicity are shown. (all data for run tg3) The vertical dashed lines, representing the transition between the different phases have been determined by using the flatness of the magnetic field (see section 4 and Fig 4).

is shown for the same simulation. When the magnetic energy attains a magnitude of the order of one percent of the kinetic energy the enstrophy drops. This drop is larger the smaller is Pr (or Rm) that is the closer one is to the dynamo onset. This rapid change of Ω marks the transition between the linear phase and the non-linear phase. The saturated regime is characterized by strong fluctuations in both energies and enstrophy. Note in Fig. 1 (right) that the normalized cross helicity h_C starts to fluctuate in the non-linear phase, showing a tendency towards an alignment of the $\boldsymbol{u}$ and $\boldsymbol{B}$ fields. We find $\langle h_C^2 \rangle^{1/2} = 0.03$ during the kinematic phase and $\langle h_C^2 \rangle^{1/2} = 0.23$ during the saturated phase. This alignment leads to a less efficient global electromotive force $\mathbf{u} \times \mathbf{b}$. In the sequel we will present another quantity whose statistics strongly changes from one regime to another and which allows for a more precise definition of the different phases of dynamo action. This quantity is in fact used to plot the vertical dashed lines in Fig. 1.

As mentioned before, the TG flow presents a manifest anisotropy coming from the very definition of the forcing. In the hydrodynamic regime we find a global isotropy coefficient $\rho_u^{iso} = 0.74$ (see table 2). Anisotropy is even enhanced to $\rho_u^{iso} \approx 0.36$ in the saturation regime, where large scale magnetic coherent structures appear in the two shear vortex plans and large tubes of kinetic energy are along the diagonal direction (see Fig. 2). We note that for the frozen force dynamo ρ_u^{iso} is close to unity during all phases of the simulation.

We now turn to the geometry of tracer trajectories. The linear phase is characterized by chaotic trajectories showing spiral motions around vorticity filaments

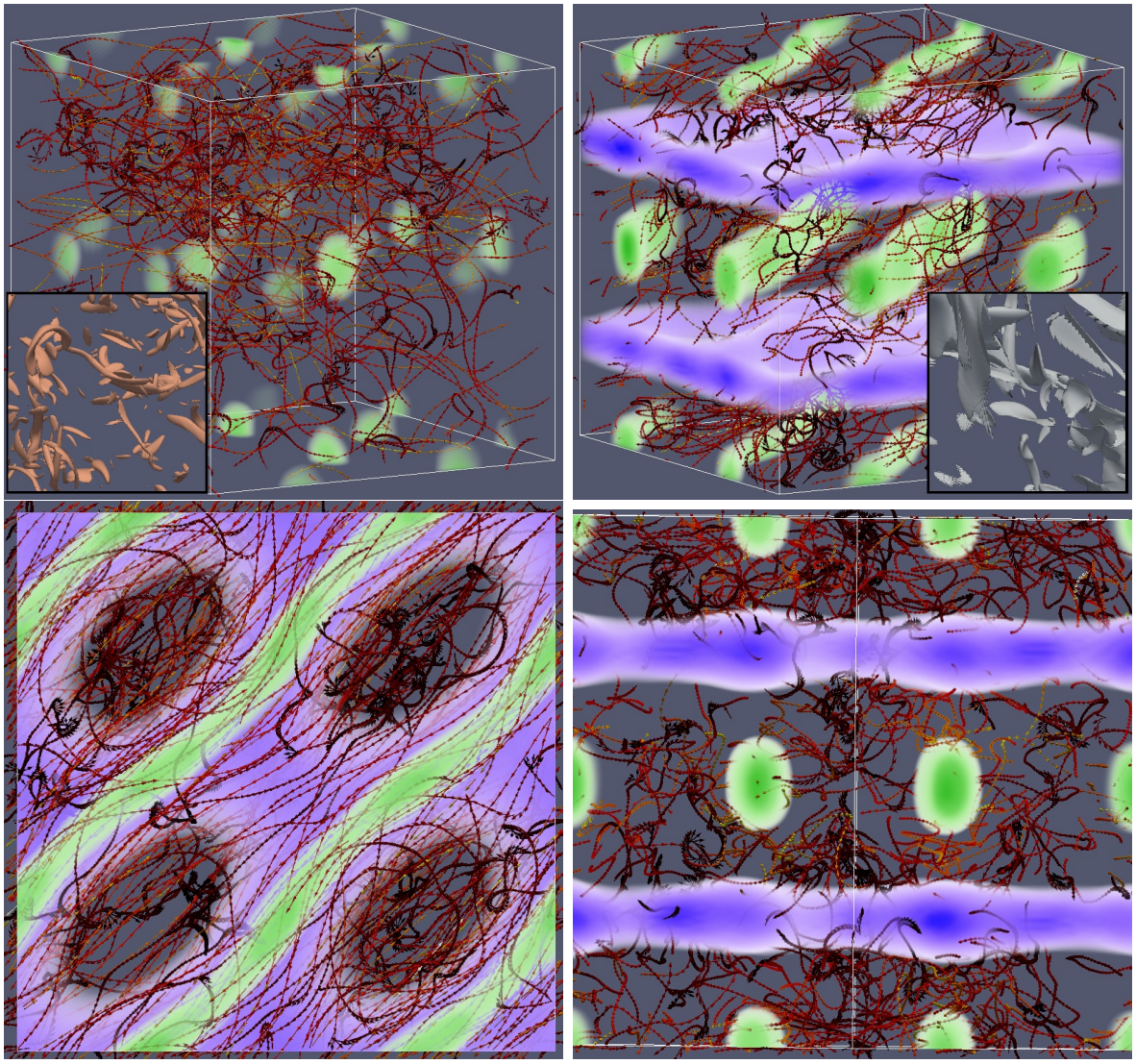


Figure 2: Volume rendering of the time-averaged kinetic energy (green) and magnetic energy (blue) for run tg3 together with tracer trajectories. Their speed is given in colors from black (low) to yellow (high). *Left top* : Linear phase. The inset shows a snapshot of the enstrophy, where vortex filaments can be observed. *Right top* : Saturated phase. The inset shows a snapshot of the en-trophy, where MHD vortex filaments and sheets are visible. *Left bottom* : Top view (along z-axis) of the saturated phase. *Right bottom* : Transverse view (along x,y-diagonal) of the saturated phase.

(see Fig. 2 (top left)) which resemble trajectories in homogeneous and isotropic turbulence. The flow is approximately homogeneous.

In the saturated phase the flow structure and the geometry of the trajectories change (see top right panel of Fig. 2). Vorticity filaments of the kinematic phase are quenched to vortex sheets in the saturated phase (see inset). The magnetic field has an ordering and smoothing effect. Trajectories become highly aligned with the structures of the

mean (time-averaged) kinetic and magnetic energy. These large-scale structures, well known in the literature, interconnect the fundamental boxes of the Taylor-Green flow. In the vicinity of the diagonally oriented high kinetic energy tubes, we observe streams of tracers with high velocities. They are separated by regions of chaotic motions (see Fig. 2 (bottom left)) which coincides with regions of low mean magnetic energy. From the bottom right panel of Fig. 2 one sees that an approximately isotropic tracers motion of the fluid is preserved perpendicular to the diagonal structures. For the frozen force (run ff), there is no large scale structure traversing the fundamental box (not shown). Blobs of increased magnetic energy are randomly distributed all over the cube. Tracer trajectories are in this case statistically homogeneous and isotropic.

4. Statistics of fluctuations

4.1. Eulerian statistics

A turbulent flow naturally leads to magnetic field fluctuations which originate from stretching, twisting and diffusion of magnetic field lines. The statistical properties of these fluctuations change significantly from one regime to another. Especially those of the magnetic field whose probability distribution functions (PDFs) are shown in Fig. 3.

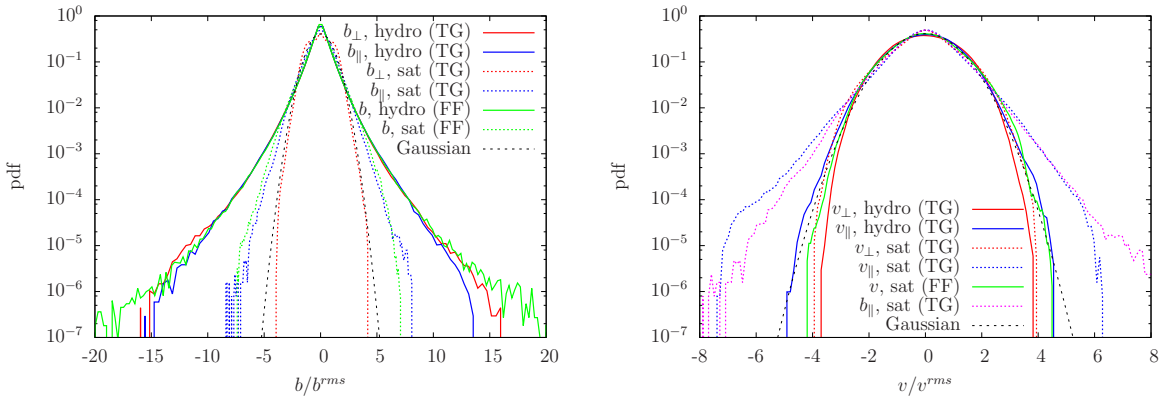


Figure 3: Probability distribution function of the magnetic field (left) and the velocity field (right) where the magnetic field component $b_\parallel, sat$ (TG) is added for comparison. The data of the saturated Taylor-Green regime is from run tg3.

In the linear phase, the PDFs of the perpendicular magnetic field components present fat tails, far away from the Gaussian distribution (Fig. 3 left). Even at moderate Reynolds numbers we observe fluctuations of the magnetic field which are 15 times larger than its root mean square value. We emphasize that this non-Gaussian character of the magnetic field during the linear phase is also observed for the frozen large scale forcing (run ffH), as apparent in Fig. 3 (left). It has also been observed by a model using the Recent Fluid Deformation closure [55]. This strongly suggests that the non-Gaussianity of the growing magnetic field is a generic property of the linear phase. In contrast,

the velocity field has nearly Gaussian statistics (see Fig. 3 right) as usually observed in hydrodynamic turbulence.

When the flow enters the saturated phase the normalized PDFs of the velocity and magnetic field components become similar. The tails of the perpendicular component $b_\perp$ of the magnetic field PDF shrink to quasi-Gaussian tails (Fig. 3 left). The perpendicular component of the velocity field $v_\perp$ remains Gaussian. Such magnetic-field PDFs along the saturated regime have also been observed in the VKS experiment [7]. The parallel component of the velocity field seems to follow the magnetic field: The PDF of $b_\parallel$ remains non-Gaussian and that of $v_\parallel$ develops non-Gaussian tails. A reason for this matching of velocity and magnetic field PDFs might be the increased alignment of v and b in the saturated regime which couples kinetic and magnetic fluctuations. Scale dependent alignment has been recently evoked in a model of the scaling properties of MHD turbulence [56].

In order to estimate the non-Gaussianity of a field f, the temporal evolution of its flatness $\langle f^4\rangle/\langle f^2\rangle^2$ is measured. The flatness of the magnetic field starts from a large value (see Fig. 4) originating from their stretched tails. During the non-linear phase its flatness strongly reduces and reaches a slightly sub-Gaussian value for the perpendicular component $b_\perp$ while it is super-Gaussian for the parallel component $b_\parallel$. A significant change can also be observed for the flatness of the velocity field PDFs (see also Fig. 4). The perpendicular component $v_\perp$ starts slightly sub-Gaussian and fluctuates around the Gaussian value 3, while the flatness of the component $v_\parallel$ is clearly larger and comparable to that of $b_\parallel$ during the saturated phase. These changes in the behavior of the flatness temporal evolution allow to clearly distinguish the three phases of the dynamo action indicated by the vertical lines drawn in Fig. 1 and 4).

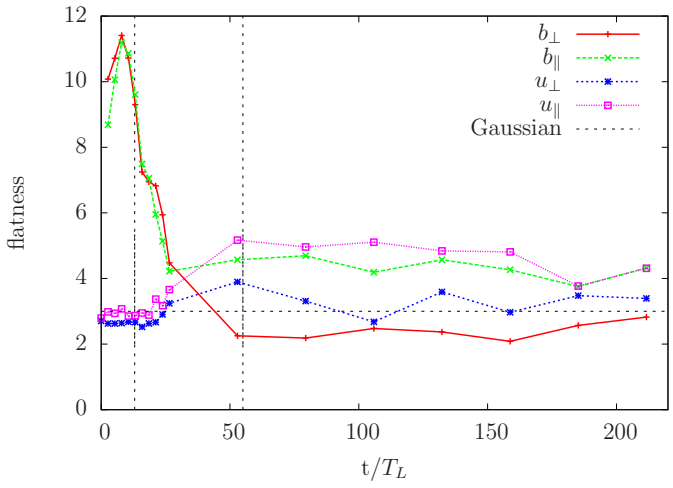


Figure 4: Temporal evolution of the flatness of the magnetic and velocity field PDFs for run tg3.

We now turn to the statistics of a small scale quantity of the flow, namely the fluid

acceleration, whose PDFs are displayed in Fig. 5 (left). Contrarily to the PDFs of the velocity, a large scale quantity, there are no significant differences among perpendicular and parallel components. This is agreement with the general observation that anisotropy of large scales decreases towards the smaller scales in turbulent flows. In order to improve statistics, the three acceleration components have been averaged. The acceleration has strongly non-Gaussian tails as usually observed in turbulent flows [57] and decrease from the kinematic to the saturated phase (see Fig. 5 (left)). This is an agreement with the known fact that the saturation regime smoothes out the small scales of the velocity. Indeed, the rms acceleration reduces from $a_{rms} = 80$ for the hydrodynamic phase to $a_{rms} = 16$ and $a_{rms} = 10$ for the saturated phase for $Pm = 1$ and $Pm = 1/4$, respectively. Smaller magnetic Prandtl numbers imply thus smaller accelerations. However, when comparing the normalized PDFs (normalized to standard deviation, Fig. 5 (right)), more extreme accelerations events are observed for the saturated regime than the pure hydrodynamic case. The tails of the PDFs become significantly fatter. The flatness of the PDFs reaches 25 in the saturated regime, while it is 14 in the hydro case. Here, the Prandtl number has a negligible effect.

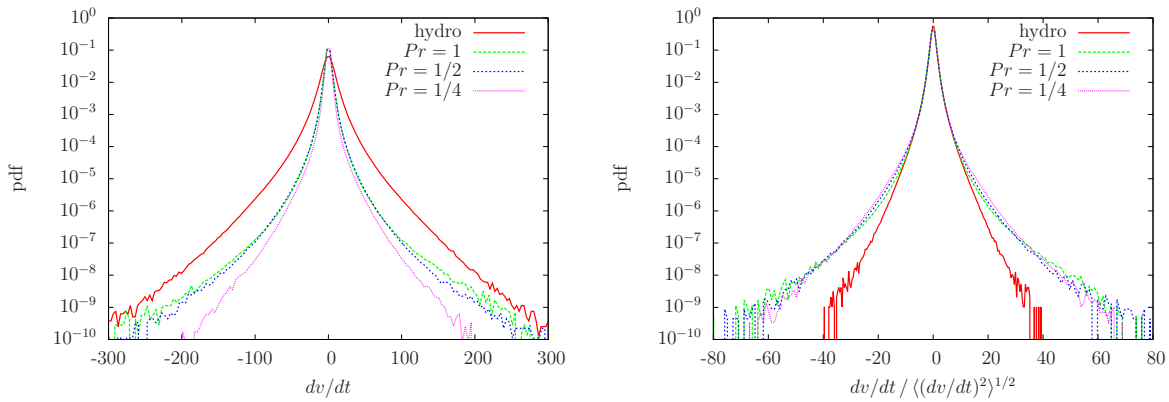


Figure 5: Probability distribution function of acceleration. Non-normalized (left) and normalized to standard deviation (right) for a hydrodynamic simulation (run tgH) and saturated regimes (run tg1, tg2, and tg3).

4.2. Lagrangian statistics

We now turn to study the properties of the magnetic field along fluid element trajectories, i.e. the magnetic field seen by a tracer. We will first focus on changes in the perpendicular component of the magnetic field, the dominant component of the mean field. For this, we consider the temporal increment $\delta b_\perp(\tau, t, \boldsymbol{x}) = B_\perp(\boldsymbol{X}(\boldsymbol{x}, t + \tau), t + \tau) - B_\perp(\boldsymbol{X}(\boldsymbol{x}, t), t)$ where $B_\perp$ denotes a magnetic field component from the perpendicular plane (B_x or B_y) and $\boldsymbol{X}(\boldsymbol{x}, t)$ a fluid trajectory starting at $\boldsymbol{x}$ at a time t. To improve statistics we average over $\boldsymbol{x}$ and t which leads to the study of the magnetic

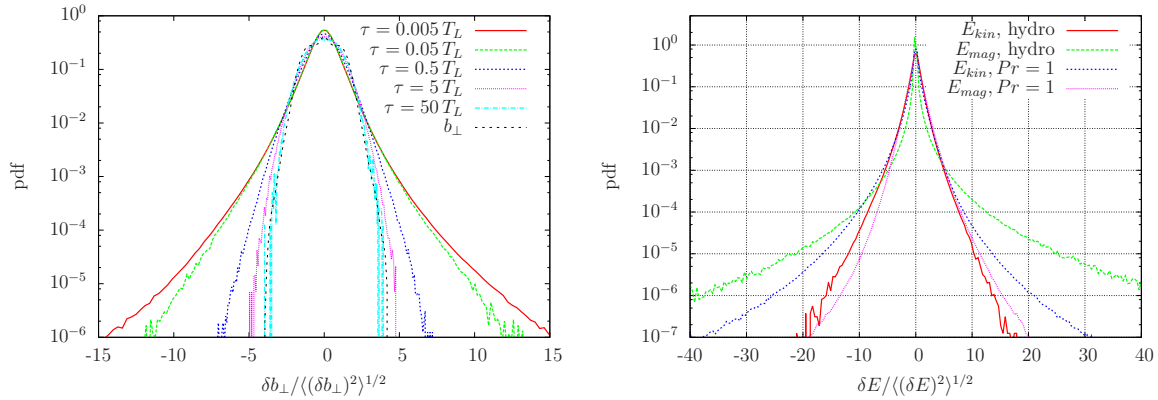


Figure 6: *Left*: PDFs of the magnetic field increments in the perpendicular direction along fluid element trajectories for several time lags in the saturated phase. For comparison the PDF of the $b_\perp$ is shown. (data from run tg3) *Right*: PDFs of the magnetic field energy increments for τ of the order of $5 \cdot 10^{-3} T_L \sim \tau_K$. (data from run tg3)

field increment

$$\delta b_\perp(\tau) = b_\perp(\tau) - b_\perp(0). \tag{7}$$

The normalized PDFs of the increment $\delta b_\perp$ during the saturated phase are shown in Fig. 6 (left). Stretched tails were also observed for small scale magnetic fluctuations in the solar wind [58]. With increasing time-lag τ the PDFs show a transition to Gaussian statistics for large time lags. This is simply due to time decorrelation of $b_\perp(\tau)$ and $b_\perp(0)$ so that one recovers for large τ the one-point Eulerian PDF shown in Fig. 3 (left). It is important to stress that the time scale τ at which this decorrelation happens is unusually long as it exceeds significantly one large-eddy turn-over time. The associated long time regime will be analyzed in detail in the subsequent section.

Another type of Lagrangian increment has recently attracted interest in the hope of a better understanding of the energy cascade and energy flux in turbulent flows [59], namely the kinetic (and magnetic) energy increment

$$\delta E_v(\tau) = \frac{1}{2}(\boldsymbol{v}^2(\tau) - \boldsymbol{v}^2(0)). \tag{8}$$

In Fig. 6 (right) the corresponding PDFs are shown for a short time lag τ. The mean of all PDFs but that of the magnetic field energy during the linear phase is zero. Only the mean of the latter is positive because of the exponential increase of magnetic energy. More interesting is their skewness $S_f = \langle f^3\rangle/\langle f^2\rangle^{3/2}$. For the hydro case the PDF of the kinetic energy has a negative skewness of $S_v \approx -0.4$. We remark that the Lagrangian derivative $d|\boldsymbol{u}|^2/dt$ can be written in terms of Eulerian quantities $d|\boldsymbol{u}|^2/dt = 2(|\boldsymbol{u}|^2\nabla^{\parallel}_{\boldsymbol{u}}\boldsymbol{u} + \boldsymbol{u}\partial_t\boldsymbol{u})$, where $\nabla^{\parallel}_{\boldsymbol{u}}\boldsymbol{u}$ is the longitudinal velocity gradient $\nabla^{\parallel}_r\boldsymbol{u} \equiv \hat{\boldsymbol{r}}\cdot(\hat{\boldsymbol{r}}\cdot\nabla\boldsymbol{u})$ evaluated in the direction of the local velocity $\hat{\boldsymbol{u}}$. $\nabla^{\parallel}_r\boldsymbol{u}$ averaged over $\hat{\boldsymbol{r}}$ is known to have negative skewness close to the one measured for

$d|\boldsymbol{u}|^2/dt$. A negative skewness means that violent decelerations are more probable than violent accelerations. The skewness of the velocity PDFs decreases towards the saturated regime ($S_v \approx -1.0$ for $Pm = 1/4$, $S_v \approx -1.2$ for $Pm = 1/2$ and $S_v \approx -1.2$ for $Pm = 1$). In contrast, the magnetic field PDF has a positive skewness $S_b \approx 2.5$ during the kinematic phase, which decreases in the saturated phase ($S_b \approx 0.43$ for $Pm = 1/4$, $S_b \approx 0.32$ for $Pm = 1/2$ and $S_b \approx 0.34$ for $Pm = 1$).

The evolution of the energy increment skewness along the different dynamo regimes, is related to the energy exchange between the kinetic and the magnetic energies in the non-linear and saturation regimes. Note that energy transfers are non-linear exchanges, with local and non local transfer in a large range of scale [60, 61].

5. Long time scaling regime

In the previous section we observed that the transition to Gaussian statistics of the perpendicular magnetic field takes very long times during the saturated regime while this happens on time scales of the order of T_L in the kinematic regime. The reason are long lasting correlations. The autocorrelation of the Lagrangian velocity increments $C_v(\tau) = \langle v_i'(t)v_i'(t+\tau)\rangle/\langle v_i'^2(t)\rangle$ with $v_i'(t) = v_i(t) - \langle v_i(t)\rangle$, is displayed in Fig. 7 (left). The Lagrangian correlation time is indeed of the order T_L for the hydrodynamic regime. During the saturated regime the perpendicular component of the velocity field remains correlated for a longer time (see Fig. 7) (left)) of the order of several T_L. Note that the parallel component becomes anti-correlated at times of the order of π/v_z^{rms} (see table 2). This corresponds to the typical time of a fluid particle crossing a TG fundamental box in the z direction and starting to feel the mirror symmetries of the TG flow.

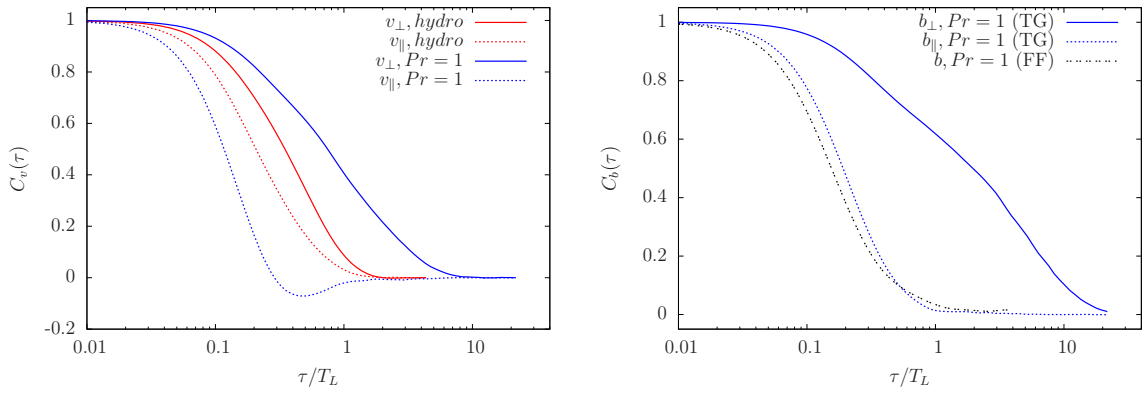


Figure 7: *Left*: Autocorrelation functions $C_v(\tau)$ of the velocity along trajectories in the hydrodynamic phase (run tgH) and saturated phase (run tg3) *Right*: Autocorrelation functions $C_b(\tau)$ of the magnetic field measured along trajectories for the saturated phase for run tg3, and ff.

The long correlation time scale is also clearly observed for the magnetic increments in Fig. 7 (right) and corresponds to the time-lag for which the PDF of the magnetic

field increments becomes Gaussian. We note that this time scale is a specific property of the TG flow which is not observed with the frozen force (run ff, Fig. 6 (right)) and it does only weakly depend on Pm.

In order to better understand the long time correlations and the non-Gaussianity of the magnetic field increments we study Lagrangian structure functions (LSF) of the form

$$S_p^B(\tau) = \langle |B_\perp(t+\tau) - B_\perp(t)|^p \rangle \tag{9}$$

during the saturated phase. Here again, $B_\perp$ denotes a magnetic field component from the perpendicular plane (B_x or B_y). In turbulent flows structure functions are usually measured to identify and to analyze the scales of the inertial range (for u_i instead of B_i) in which they behave as a power law $S_p(\tau) \sim \tau_p^\zeta$. The corresponding scaling exponents ζ_p provide a handle on the phenomenon of intermittency which characterizes the occurrence of extreme events in the dynamical evolution of the system [62].

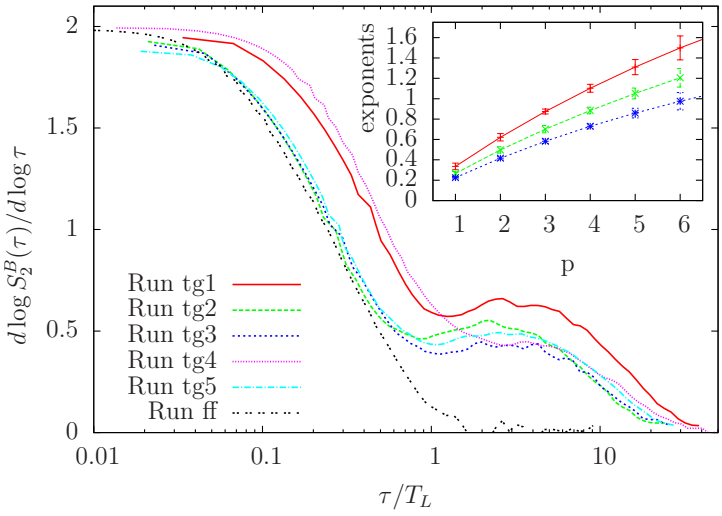


Figure 8: Local slope of the second order Lagrangian structure functions of the magnetic field $S_2^B(\tau)$ for all runs in the saturated regime. The inset shows the measured scaling exponents ζ_p^B different orders p. Error bars give the maximal variation around the mean in the interval where S_2^B is flat. (data from run tg1, tg2, and tg3)

A scaling range and corresponding scaling exponents can reliably be measured via the local slope of the structure functions that is their logarithmic derivative $d \log S_p / d \log \tau$. This quantity for the second order LSF S_2^B is shown in Fig 8 for all runs. In hydrodynamic turbulence, even for very large Reynolds numbers, the range of scales where a power law is observed and where thus the local slope is constant is very narrow if visible at all [63]. We therefore do not expect to observe a power-law behavior on time-scales shorter than $1\,T_L$. Surprisingly, for larger times scales we observe a clear plateau for the Taylor-Green runs. Its width is similar (from approximately $1\,T_L$ to $10\,T_L$) for all runs but run tg4 (forced at $k_0 = 2$) indicating a relationship with the

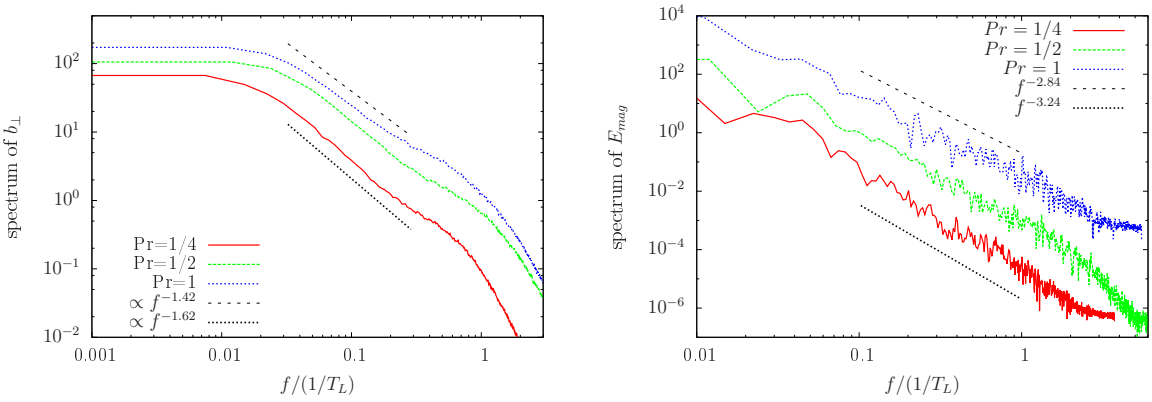


Figure 9: Left: Power density spectrum (PDS) of $b_\perp$ for run tg1, tg2, and tg3. The frequency f is given in terms of the large scale frequency $1/T_L$. Right: PDS of the total magnetic energy $E_{\rm mag}(t)$ for run tg1, tg2, and tg3. All curves are shifted for clarity.

forcing. The corresponding scaling exponent does not seem to depend on the Reynolds number of the flow while it changes depending on the magnetic Prandtl number: It decreases with increasing Pm. As expected, for the frozen-force simulation (ff) where correlations do not persist beyond $1\,T_L$ no scaling region is observed.

Higher order statistics reveal that the magnetic fluctuations in this scaling region are intermittent. The scaling exponents ζ_p^B of the structure functions S_p^B up to order six are shown in the inset of Fig. 8 for three different Prandtl numbers. They reveal that the long time magnetic fluctuation are intermittent as all curves are bended. Concerning their magnetic Prandtl number dependence one finds that the values of the exponents grow with decreasing Pm but we note that the curves of the relative scaling exponents ζ_p/ζ_2 fall on top of each other within the error bars (not shown).

In order to better understand the origin of the observed long time correlations we computed the auto-correlations of the terms on the right hand side of (1) multiplied by $\boldsymbol{u}$. They corresponds to the correlation of the energy sources and sinks of the velocity field. We find that the correlation time of the mean external energy injection rate $\langle \boldsymbol{u}\cdot\boldsymbol{F}\rangle$ becomes longer during the non-linear phase and extends well beyond one T_L during the saturated phase. It is then also on this time scale that the total energy of the system fluctuates. This is in agreement with the observed changes of the correlation time of $u_\perp$ in Fig. 7 (left) as the Taylor-Green force is constant. The energy exchange time scale $\langle \boldsymbol{u}\cdot(\nabla\times\boldsymbol{B})\times\boldsymbol{B}\rangle$ connected to the Lorentz force is shorter. We note that the mean external energy injection rate is a large-scale quantity. Apparently, the Lorentz force changes the global flow structure in such a way that the resulting large-scale velocity field and the (constant) Taylor Green force remain correlated for times much longer than without Lorentz force. The observed scaling regime is probably not a classical turbulent scaling regime.

We complement the discussion of the long time scaling regime by analyzing the

power density spectrum (PDS) of the perpendicular magnetic field $b_\perp$ along tracer trajectories. For the PDS we find a low frequency band showing a power-law decay (see Fig. 9 (left)). The slope ζ_2 of a second order structure function and that of the corresponding PDS (α) are connected via the formula $\alpha = -\zeta_2 - 1$ [62]. The measured slopes of the PDS are consistent with the scaling exponents of the structure functions.

Finally, we would like to note that we measured slopes of the spectrum of the temporal fluctuations of the total magnetic energy $E_{\rm mag}(t)$ (see Fig. 9 (right)) which are compatible with the previously presented data. Keeping in mind that the variable of measured PDS has a dimension of B^2 and not of B like that of the LSF we find an agreement with ζ_2^L by simple dimensional arguments.

6. Conclusions

By means of direct numerical simulations of the magnetohydrodynamic equations forced by the Taylor-Green vortex we analyzed Lagrangian statistics during the three stages of a dynamo system: the kinematic phase with negligible magnetic field energy, the non-linear phase with awakening Lorentz force, and the saturated phase when the non-linear dynamics lead to a statistically stationary equilibrium.

Lagrangian data allows for a clear identification of these three regimes. The statistics of the magnetic and the velocity field changes drastically from one phase to another. The magnetic field PDFs are strongly non-Gaussian in the kinematic phase and quasi-Gaussian in the saturated regime. PDFs of magnetic and velocity energy increments along tracer trajectories are skewed. We find a positive skewness for the magnetic energy which reduces from the kinematic to the saturated phase. The skewness of the kinetic energy is negative during the kinematic phase and is even smaller during the saturated phase. The evolution of the skewness of PDF energy increment is clearly due the energy transfer between the kinetic and magnetic energies.

Temporal correlations extend much longer in the saturated regime than in the kinematic one and exceed significantly one large-eddy turn-over time. This is in agreement with increased temporal correlations of the external kinetic energy injection rate due to the action of the Lorentz force. Remarkably, we find a clear scaling regime of magnetic field increments along particle trajectories at time scales approximately ranging from one to ten large-eddy turn-over times. High-order scaling exponents of the Lagrangian structure functions show that these long-time magnetic field fluctuations are intermittent. The second-order scaling is consistent with a power-law observed for the corresponding frequency spectrum and that of fluctuations of the total magnetic energy of the system.

Finally, we would like to briefly mention that we do not observe a long time scaling regime for simulations with an ABC force. If it is specific to the Taylor-Green force or if also other forces develop it has to be investigated in future work.

Acknowledgments

We thank J.F. Pinton for useful discussions. Access to the IBM BlueGene/P computer JUGENE at the FZ Jülich was made available through project HBO22 and partly through project HBO36. Computer time was also provided by GENCI and the Mesocentre SIGAMM machine. This work benefited from support through DFG-FOR1048

[1] A. Gailitis, O. Lielausis, S. Dement'ev, E. Platacis, A. Cifersons, G. Gerbeth, T. Gundrum, F. S. M. Christen, H. H. anel, and G. Will, "Detection of a flow induced magnetic field eigenmode in the riga dynamo facility," *Phys. Rev. Lett.*, vol. 84, p. 4365, 2000.

[2] A. Gailitis, O. Lielausis, S. Dement'ev, A. Cifersons, G. Gerbeth, T. Gundrum, F. S. M. Christen, H. H. anel, and G. Will, "Magnetic field saturation in the riga dynamo experiment," *Phys. Rev. Lett.*, vol. 86, p. 3024, 2001.

[3] U. Müller and R. Stieglitz, "Can the earth's magnetic field be simulated in the laboratory?," *Naturwissenschaften*, vol. 87, p. 381, 2000.

[4] R. Stieglitz and U. Müller, "Experimental demonstration of a homogeneous two-scale dynamo," *Phys. Fluids*, vol. 13, p. 561, 2001.

[5] R. Monchaux, M. Berhanu, M. Bourgoin, M. Moulin, P. Odier, J. Pinton, R. Volk, S. Fauve, N. Mordant, F. Pétrélis, A. Chiffaudel, F. Daviaud, B. Dubrulle, C. Gasquet, L. Marié, and F. Ravelet, "Generation of a magnetic field by dynamo action in a turbulent flow of liquid sodium," *Phys. Rev. Lett.*, vol. 98, p. 044502, 2007.

[6] M. Berhanu, R. Monchaux, S. Fauve, N. Mordant, F. Pétrélis, A. Chiffaudel, F. Daviaud, F. Ravelet, M. Bourgoin, P. Odier, J.-F. Pinton, R. Volk, B. Dubrulle, and L. Marié, "Magnetic field reversals in an experimental turbulent dynamo," *Europhys. Lett.*, vol. 77, p. 59001, 2007.

[7] R. Monchaux, M. Berhanu, S. Aumaitre, A. Chiffaudel, F. Daviaud, B. Dubrulle, F. Ravelet, S. Fauve, N. Mordant, F. Petrelis, M. Bourgoin, P. Odier, J. Pinton, N. Plihon, and R. Volk, "The von kármán sodium experiment: Turbulent dynamical dynamos," *Phys. Fluids*, vol. 21, pp. 035108–21, 2009.

[8] M. Berhanu, B. Gallet, R. Monchaux, M. Bourgoin, P. Odier, J. Pinton, N. Plihon, R. Volk, S. Fauve, N. Mordant, F. Pétrélis, S. Aumaître, A. Chiffaudel, F. Daviaud, B. Dubrulle, and F. Ravelet, "Bistability between a stationary and an oscillatory dynamo in a turbulent flow of liquid sodium," *Journ. Fluid Mech.*, vol. 641, pp. 217–226, 2009.

[9] M. Berhanu, G. Verhille, J. Boisson, B. Gallet, C. Gissinger, S. Fauve, N. Mordant, F. Pétrélis, M. Bourgoin, P. Odier, J. Pinton, N. Plihon, S. Aumaître, A. Chiffaudel, F. Daviaud, B. Dubrulle, and C. Pirat, "Dynamo regimes and transitions in the VKS experiment," *The European Physical Journal B*, vol. 77, pp. 459–468, 2010.

[10] B. Gallet, S. Aumaître, J. Boisson, F. Daviaud, B. Dubrulle, N. Bonnefoy, M. Bourgoin, P. Odier, J.-F. Pinton, N. Plihon, G. Verhille, S. Fauve, and F. Pétrélis, "Experimental observation of spatially localized dynamo magnetic fields," *Phys. Rev. Lett.*, vol. 108, p. 144501, 2012.

[11] S. Childress and A. Gilbert, *Stretch, Twist, Fold: The Fast Dynamo*. Berlin: Springer-Verlag, 1995.

[12] Y. Ponty, P. Minnini, J.-F. Pinton, H. Politano, and A. Pouquet, "Dynamo action at low magnetic prandtl numbers: mean flow versus fully turbulent motions," *New Journal of Physics*, vol. 9, p. 296, 2007.

[13] Y. Ponty and F. Plunian, "Transition from large-scale to small-scale dynamo," *Phys. Rev. Lett.*, vol. 106, p. 154502, 2011.

[14] B. Dubrulle, P. Blaineau, O. L. Mafra, F. Daviaud, J. Laval, and R. Dolganov, "Bifurcations and dynamo action in a taylor-green flow," *New Journal of Physics*, vol. 9, no. 8, p. 308, 2007.

[15] A. A. Schekochihin, A. B. Iskakov, S. C. Cowley, J. C. McWilliams, M. R. E. Proctor, and T. A. Yousef, "Fluctuation dynamo and turbulent induction at low magnetic prandtl numbers," *New J. Phys.*, vol. 9, p. 300, 2007.

[16] F. Cattaneo, D. Hughes, and E. Kim, "Suppression of chaos in a simplied nonlinear dynamo model," *Phys. Rev. Lett.*, vol. 76, pp. 2057–2060, 1996.

[17] E. Zienicke, H. Politano, and A. Pouquet, "Variable intensity of lagrangian chaos in the nonlinear dynamo problem.," *Phys. Rev. Lett.*, vol. 81, pp. 4640–4640, 1998.

[18] J. Pinton and Y. Ponty, "Private communication." In Roma airport back from a conference in Catania, October 2007.

[19] F. Toschi and E. Bodenschatz, "Lagrangian properties of particles in turbulence," *Ann. Rev. of Fluid Mech.*, vol. 41, pp. 375–404, 2009.

[20] L. Biferale, G. Boffetta, A. Celani, B. J. Devenish, A. Lanotte, and F. Toschi, "Multifractal statistics of lagrangian velocity and acceleration in turbulence," *Phys. Rev. Lett.*, vol. 93, no. 6, p. 4502, 2004.

[21] P. K. Yeung and M. S. Sawford, "Reynolds number dependence of lagrangian statistics in large numerical simulations of isotropic turbulence," *J. of Turbulence*, vol. 7, pp. 1–12, 2006.

[22] J. Bec, L. Biferale, G. Boffetta, A. Celani, M. Cencini, A. Lanotte, S. Musaccio, and F. Toschi, "Acceleration statistics of heavy particles in turbulence," *Journ. Fluid Mech.*, vol. 550, pp. 349–358, 2006.

[23] P. K. Yeung and M. S. Borgas, "Relative dispersion in isotropic turbulence. part 1. direct numerical simulations and reynolds-number dependence," *Journ. Fluid Mech.*, vol. 503, pp. 93–124, 2004.

[24] R. Bitane, H. Homann, and J. Bec, "Geometry and violent events in turbulent pair dispersion," *J. of Turbulence*, vol. 14, pp. 23–45, 2013.

[25] G. Eyink, E. Vishniac, C. Lalescu, H. Aluie, K. Kanov, K. Bürger, R. Burns, C. Meneveau, and A. Szalay, "Flux-freezing breakdown in high-conductivity magnetohydrodynamic turbulence," *Nature*, vol. 497, pp. 466–469, 2013.

[26] N. Mordant, P. Metz, O. Michel, and J.-F. Pinton, "Measurement of lagrangian velocity in fully developed turbulence," *Phys. Rev. Lett.*, vol. 87, p. 214501, 2001.

[27] N. Mordant, J. Delour, E. Léveque, A. Arnéodo, and J.-F. Pinton, "Long time correlations in lagrangian dynamics: A key to intermittency in turbulence," *Phys. Rev. Lett.*, vol. 89, p. 254502, 2002.

[28] A. La Porta, G. A. Voth, F. Moisy, and E. Bodenschatz, "Using cavitation to measure statistics of low-pressure events in large-reynolds-number turbulence," *Phys. Fluids*, vol. 12, pp. 1485–1496, 2000.

[29] A. La Porta, G. A. Voth, A. M. Crawford, J. Alexander, and E. Bodenschatz, "Fluid particle accelerations in fully developed turbulence," *Nature*, vol. 409, pp. 1017–1019, 2001.

[30] H. Homann, R. Grauer, A. Busse, and W. C. Müller, "Lagrangian statistics of navier-stokes and mhd turbulence," *Journ. Plasma Phys.*, vol. 73, no. 06, pp. 821–830, 2007.

[31] H. Homann, O. Kamps, R. Friedrich, and R. Grauer, "Bridging from eulerian to lagrangian statistics in 3d hydro and magnetohydrodynamic turbulent flows," *New Journ. Phys.*, vol. 11, p. 073020, 2009.

[32] A. Celani, A. Mazzino, and D. Vincenzi, "Magnetic field transport and kinematic dynamo effect: a Lagrangian interpretation," *Proc. R. Soc. A*, vol. 462, pp. 137–147, 2006.

[33] M. E. Brachet, D. I. Meiron, S. A. Orszag, B. G. Nickel, R. H. Morf, and U. Frisch, "Small-Scale structure of the Taylor-Green vortex," *Journ. Fluid Mech.*, vol. 130, pp. 411–452, 1983.

[34] C. Nore, M. Brachet, H. Politano, and A. Pouquet, "Dynamo action in the taylor–green vortex near threshold," *Phys. Plasmas*, vol. 4, p. 1, 1997.

[35] C. Nore, M.-E. Brachet, H. Politano, and A. Pouquet, "Dynamo action in a forced taylor-green vortex," *Dynamo and Dynamics, a mathematical challenge, Nato Science Series II, Vol. 26, edited by P. Chossat, D. Armbruster and I. Oprea (Kluwer Academic, Dordrecht, Proceedings of the Nato Advanced Research Workshop, Cargèse, France, 21-26 August 2000*, pp. 51–58, 2001.

[36] Y. Ponty, P. M. A. Pouquet, H. Politano, D. Montgomery, and J. Pinton, "Numerical study of dynamo action at low magnetic prandtl numbers," *Phys. Rev. Lett.*, vol. 94, p. 164512, 2005.

[37] P. D. Mininni, Y. Ponty, D. C. Montgomery, J.-F. P. H. Politano, and A. Pouquet, "Dynamo

regimes with a non-helical forcing," *The Astrophysical Journal*, vol. 626, pp. 853–863, 2005.

[38] Y. Ponty, P. D. Mininni, J.-P. Laval, A. Alexakis, J. Baerenzung, F. Daviaud, B. Dubrulle, J.-F. Pinton, H. Politano, and A. Pouquet, "Linear and non linear features of the taylor-green dynamo," *C. R. Physique*, vol. 9, pp. 749–756, 2008.

[39] G. Krstulovic, G. Thorner, J.-P. Vest, S. Fauve, and M. Brachet, "Axial dipolar dynamo action in the taylor-green vortex," *Phys. Rev. E*, vol. 84, p. 066318, 2011.

[40] D. Dijkstra and G. J. F. V. Heijst, "The flow between two finite rotating disks enclosed by a cylinder," *Journ. Fluid Mech.*, vol. 128, pp. 123–154, 1983.

[41] S. Douady, Y. Couder, and M. E. Brachet, "Direct observation of the intermittency of intense vorticity filaments in turbulence," *Phys. Rev. Lett*, vol. 67, pp. 983–986, 1991.

[42] S. Fauve, C. Laroche, and B. Castaing, "Pressure fluctuations in swirling turbulent flows," *Journal de Physique II*, vol. 3, pp. 271–278, mar 1993.

[43] R. L. J.-F. Pinton, "Correction to taylor hypothesis in swirling flows," *Journal de Physique II (France)*, vol. 4, pp. 1461–1468, 1994.

[44] P. Abry, S. Fauve, P. Flandrin, and C. Laroche, "Analysis of pressure fluctuations in swirling turbulent flows," *Journal de Physique II*, vol. 4, pp. 725–733, May 1994.

[45] R. Labbé, J.-F. Pinton, and S. Fauve, "Study of the von kàrmàn flow between coaxial corotating disks," *Phys. Fluids*, vol. 8, pp. 914–922, Apr. 1996.

[46] O. Cadot, Y. Couder, A. Daerr, S. Douady, and A. Tsinober, "Energy injection in closed turbulent flows: Stirring through boundary layers versus inertial stirring," *Physical Review E*, vol. 56, p. 427, July 1997.

[47] A. de la Torre and J. Burguete, "Slow dynamics in a turbulent von kàrmàn swirling flow," *Phys. Rev. Lett.*, vol. 99, pp. 054101–4, 2007.

[48] L. Marié, *Transport de moment cinétique et de champ magnétique par un écoulement tourbillonnaire turbulent: Influence de la Rotation*. THESE, Université Paris-Diderot - Paris VII, Sept. 2003.

[49] L. Marié and F. Daviaud, "Experimental measurement of the scale-by-scale momentum transport budget in a turbulent shear flow," *Phys. Fluids*, vol. 16, p. 457, 2004.

[50] F. Ravelet, L. Marié, A. Chiffaudel, and F. c. Daviaud, "Multistability and memory effect in a highly turbulent flow: Experimental evidence for a global bifurcation," *Phys. Rev. Lett.*, vol. 93, p. 164501, 2004.

[51] F. Ravelet, *Bifurcations globales hydrodynamiques et magnetohydrodynamiques dans un ecoulement de von Karman turbulent*. THESE, 2005.

[52] F. Ravelet, A. Chiffaudel, and F. Daviaud, "Supercritical transition to turbulence in an inertially driven von kármán closed flow," *Journ. Fluid Mech.*, vol. 601, pp. 339–364, 2008.

[53] H. Homann, D. Schulz, and R. Grauer, "Conditional eulerian and lagrangian velocity increment statistics of fully developed turbulent flow," *Phys. Fluids*, vol. 23, p. 055102, 2011.

[54] H. Homann, J. Dreher, and R. Grauer, "Impact of the floating-point precision and interpolation scheme on the results of dns of turbulence by pseudo-spectral codes," *Comput. Phys. Comm.*, vol. 177, pp. 560–565, 2007.

[55] T. Hater, H. Homann, and R. Grauer, "Lagrangian model for the evolution of turbulent magnetic and passive scalar fields," *Phys. Rev. E*, vol. 83, p. 017302, 2011.

[56] S. Boldyrev, "Spectrum of magnetohydrodynamic turbulence," *Phys. Rev. Lett.*, vol. 96, p. 115002, 2006.

[57] A. L. Porta, G. A. Voth, A. M. Crawford, J. Alexander, and E. Bodenschatz, "Fluid particle accelerations in fully developed turbulence," *Nature*, vol. 409, pp. 1017–1019, 2001.

[58] O. Alexandrova, V. Carbone, P. Veltri, and L. Sorriso-Valvo, "Small-scale energy cascade of the solar wind turbulence," *The Astrophys. Journ.*, vol. 674, p. 1153, 2008.

[59] H. Xu, A. Pumir, G. Falkovich, E. Bodenschatz, M. Shats, H. Xia, N. Francois, G. Boffetta, "Power Fluctuations and Irreversibility in Turbulence", *arXiv:1310.5006*, 2013.

[60] A. Alexakis, P. D. Mininni, and A. Pouquet, "Shell-to-shell energy transfer in magnetohydrody-

namics. i. steady state turbulence," *Phys. Rev. E*, vol. 72, p. 046301, 2005.
[61] P. Mininni, A. Alexakis, and A. Pouquet, "Shell-to-shell energy transfer in magnetohydrodynamics. II. kinematic dynamo," *Phys. Rev. E*, vol. 72, p. 046302, 2005.
[62] U. Frisch, *Turbulence*. Cambridge: Cambridge University Press, 1995.
[63] G. Falkovich, H. Xu, A. Pumir, E. Bodenschatz, L. Biferale, G. Boffetta, A. Lanotte, and F. Toschi, "On lagrangian single-particle statistics," *Phys. Fluids*, vol. 24, p. 055102, 2012.